The Astrophysical Journal, 805:84 (9pp), 2015 May 20 doi:10.1088/0004-637X/805/1/84

ON THE ORIGIN OF HIGHLY ALFVÉNIC SLOW SOLAR WIND

R. D'Amicis and R. Bruno
INAF—Institute for Astrophysics and Space Planetology, Via del Fosso del Cavaliere, I-100 Rome, Italy; raffaella.damicis@iaps.inaf.it
Received 2014 December 11; accepted 2015 March 14; published 2015 May 21

ABSTRACT

Alfvénic fluctuations are a common feature in the solar wind and are found especially in the trailing edges of fast wind streams. The slow wind usually has a lower degree of Alfvénicity, being more strongly intermixed with structures of non-Alfvénic nature. In the present paper we show the first evidence in the interplanetary space of two different kinds of slow solar wind: one coming from coronal streamers or active regions and characterized by non-Alfvénic structures and the other one being highly Alfvénic and originating from the boundary of coronal holes. The Alfvénic character of fluctuations, either outward or inward, can be studied by means of the normalized cross-helicity, σ_C, which is an indicator of the $\boldsymbol{v} - \boldsymbol{b}$ alignment. The evolution of σ_C toward lower values with increasing radial distance is interpreted both as a decrease of the presence of the outward modes and as a continuous production of inward modes within those regions such as stream shears where some plasma instability is active. On the other hand, the decrease of σ_C is often related also to magnetic field and/or density enhancements which specifically act on the destruction of the $\boldsymbol{v} - \boldsymbol{b}$ alignment. In the present analysis we study the role of compressibility presenting both case studies and a statistical analysis over different phases of solar cycle 23. Our findings indicate that the presence of regions of magnetic field compression generally play a major role in the depletion of σ_C and thus in the destruction of the $\boldsymbol{v} - \boldsymbol{b}$ alignment.

Key words: methods: data analysis – solar wind – turbulence

1. INTRODUCTION

At scales less than a few hours, the inner heliosphere is largely permeated by Alfvénic fluctuations (Belcher & Davis 1971) which propagate in a medium characterized by a well-developed Kolmogov-like turbulence (Coleman 1968). Previous studies of Alfvénic fluctuations in the solar wind, using measurements made by spacecraft in the ecliptic plane, showed that the purest examples occur in the trailing edges of fast solar wind streams (Belcher & Davis 1971) that flow from coronal holes (Hundhausen 1972; Phillips et al. 1995). The slow wind usually has a smaller amplitude than the fast stream and tends to be less pure in the sense that it is more strongly intermixed with structures of non-Alfvénic nature.

It is worth recalling that Alfvénic fluctuations in the solar wind are usually a mixture of two different populations, characterized by opposite directions of propagation in the wind plasma frame of reference. The first population, dominant in the great majority of cases, is made up of fluctuations propagating away from the Sun (outward population), while the second population is made up of fluctuations propagating toward the Sun (inward population). The Alfvénic radius is the critical distance where the solar wind becomes super-Alfvénic. This distance moves systematically from about 15 R_S at solar minimum to 30 R_S at solar maximum (Goelzer et al. 2014). Obviously, outside the Alfvénic critical point, both kinds of fluctuation are convected outwards, as seen from the Sun. The major source for outward fluctuations seen in the interplanetary space is the Sun, with smaller contributions from interplanetary sources. Conversely, interplanetary inward fluctuations can only come from sources in regions outside the Alfvénic critical point (in fact, inside this point inward waves fall back to the Sun). As it is well known (e.g., Dobrowolny et al. 1980), the presence of these two kinds of waves is a condition that leads to the development of nonlinear interactions. In fact, during the solar wind expansion, Alfvén waves outwardly propagating experience superposition with inwardly propagating Alfvén waves locally generated by velocity shears through plasma instabilities (Bavassano & Bruno 1989b). Their nonlinear interaction is then crucial for the dynamical evolution of the MHD spectrum toward a Kolmogorov-like spectrum.

Actually, the solar wind turbulence shows a high degree of Alfvénicity, namely, a high correlation between velocity and magnetic field components, and equipartition between the kinetic and magnetic energies. Such a state is realized, in particular, in the region near the Sun. Bruno et al. (2007) found that the turbulent population is largely dominated by Alfvénic fluctuations in the fast wind at 0.29 AU (at *Helios* perihelion). The same authors showed that, as the wind expands, the Alfvénic content of these fluctuations decreases and a newborn population, characterized by lower values of Alfvénicity and a clear imbalance in favor of magnetic energy, becomes visible and clearly distinguishable from the Alfvénic population. The previous results have been interpreted considering solar wind fluctuations mainly as a mixture of Alfvénic fluctuations that propagate and structures advected by the wind, as widely reported in the literature (e.g., Tu & Marsch 1993; Bruno & Carbone 2013). As the wind expands, Alfvénic fluctuations are depleted and structures become dominant.

The study of the radial evolution of Alfvénic fluctuations based on the investigation of the behavior of the normalized cross-helicity, σ_C (defined as $2v \cdot b/(E_v + E_b)$, where v and b are velocity and magnetic field respectively, and E_v and E_b are the kinetic and magnetic energy, respectively), has shown a tendency of this parameter to go toward lower values with increasing heliocentric distance (Matthaeus & Goldstein 1982; Roberts et al. 1987a, 1987b; Grappin & Velli 1996; Bavassano et al. 2000; Matthaeus et al. 2004). This evidence was interpreted as an increase in the production of the inward modes within those regions such as stream shears where some plasma instability is active. Although Bavassano & Bruno (1989b) found reasonable evidence for local generation by velocity shear, they also showed that a decrease of σ_C is closely

related to magnetic field and/or density enhancements most of the time (Bavassano & Bruno 1989a). They argued that the lack of Alfvénicity in the fluctuations rather than the local generation of inward modes would often cause the observed decrease of σ_c. This result was then also confirmed on a statistical basis by Bruno & Bavassano (1991).

The present study investigates the role played by magnetic field compression by means of case studies and is also a statistical study motivated by a recent work by D'Amicis et al. (2011) which found that solar cycle 23 shows a very peculiar behavior as will be seen in the next sections.

The outline of this paper is as follows. In Section 2 we present a case study using *Helios* 2 measurements. Sections 3 is devoted to the presentation of the statistical analysis during different phases of solar cycle 23. In Section 4 we focus our attention on the origin of the slow solar wind, while in Section 5 we investigate the role of compressibility in the evolution of solar wind Alfvénicity. Section 6 summarizes our results.

2. CASE STUDY—*HELIOS 2*

For the case study, we use *Helios 2* magnetic field and plasma data at 81 s resolution. The time intervals studied occur in 1976, during which the same fast wind stream coming from the same source region was observed at three heliocentric distances after three successive solar rotations (Bavassano et al. 1982). In this way, it is possible to study the radial evolution of solar wind features spanning distances from 0.29 to 1 AU.

Figure 1 shows the time series of the wind speed $V_{\rm sw}$ (black), the strength of B (green) and proton number density n_p (purple), and the z component of the velocity v_z and magnetic field (in Alfvén units) v_{az} in blue and red in SE coordinates, respectively, at three heliocentric distances. The z component was chosen to make results clearer since this component is found to be more Alfvénic than the x and y components (Tu et al. 1989). At 0.3 AU the solar wind speed profile is characterized by a transition from slow to fast wind occuring after two large velocity shears of the order of about 100 km s^{-1} at DoY 103.58 and 103.7. Very good Alfvénic correlations characterize the trailing edge of the fast wind and extend even in the slow wind region, preceding it for about 10 hours. Actually, Alfvénic correlations begin to develop at about DoY 103.09 when we observe an abrupt discontinuity separating two different plasma regions as will be discussed in the next figure. After crossing this discontinuity, magnetic field and density show a rather reduced compressibility. These findings suggest that density and magnetic field fluctuations rather than velocity shears act in destroying Alfvénic correlations. As a matter of fact, these correlations are lost when large density and magnetic field fluctuations are present.

The region just ahead of the fast wind, where dynamical interaction between fast and slow wind develops, is characterized by compressive effects highlighted by enhancements in proton density, temperature, and magnetic field intensity. However, this compressive region is not due to the dynamical interactions between fast and slow wind since it lies well ahead of the expected location of the interaction region. The anticorrelation between field intensity and plasma density suggests that this region might be in a quasi-pressure-balanced state (see Figure 1 in Bavassano et al. 1997). As we move away from the Sun its spatial extension becomes wider, compression is built up (see Figure 3 in Bavassano et al. 1997),

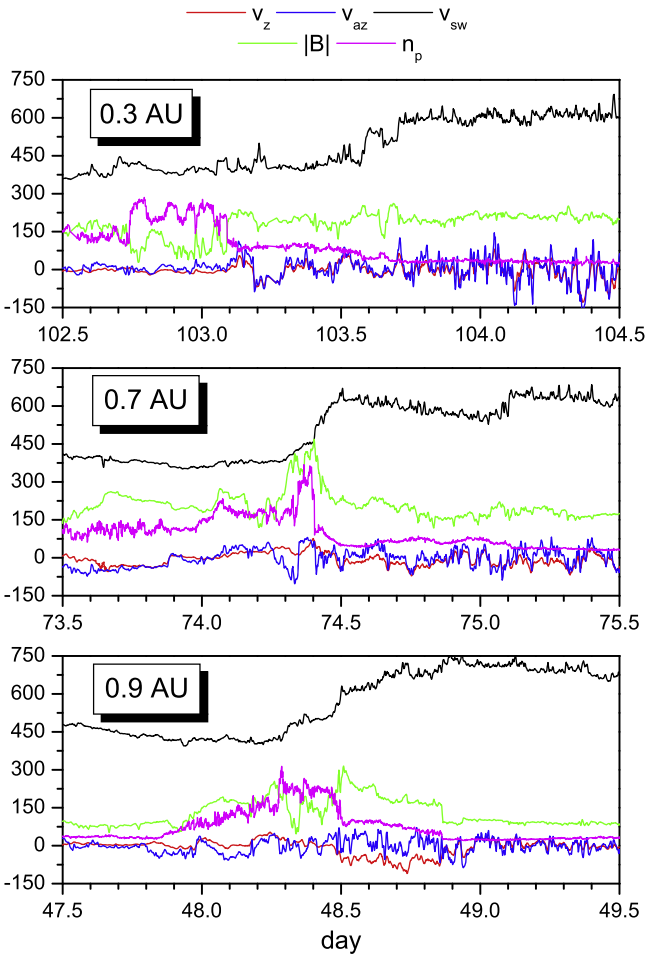

Figure 1. Time series of solar wind speed $V_{\rm sw}$ in km s^{-1} (black), magnetic field magnitude B in nT (green), proton number density n_p in cm^{-3} (purple), SE z components of velocity v_z in km s^{-1} (red) and magnetic field in Alfvén units v_{az} in km s^{-1} (blue) of a fast wind stream coming from the same source region and observed at three heliocentric distances after three successive solar rotations. B and n_p are multiplied by an arbitrary factor.

and the compressive front, which has its highest level right at the stream interface when *Helios* is at 0.7 AU, goes well beyond the stream interface by the time the stream has reached 0.9 AU. As expected, Alfvénic correlations characterize the trailing edge of the fast stream even at 0.7 and 0.9 AU. Contrary to the case at 0.3 AU, Alfvénic correlations begin well inside the fast stream and also do not involve the slow wind preceding it. In fact, correlations are less pure or almost disappear when a magnetic field and density enhancement is observed.

Figure 2 focuses on the perihelion passage and, from the top to the bottom panel, shows solar wind speed, number density and magnetic field strength, the z components of the magnetic field and velocity, and the correlation coefficient computed at 1 hr scale, respectively. Within the slow wind, the density enhancement preceding the fast wind stream, located at about DoY 102.7, identifies the heliospheric current sheet which originates from the near-equatorial belt of coronal streamers and extends into the interplanetary space dividing the heliosphere into two regions of opposite magnetic field polarity (Bavassano et al. 1997). These authors found a clear correspondence between the profile of the path-integrated

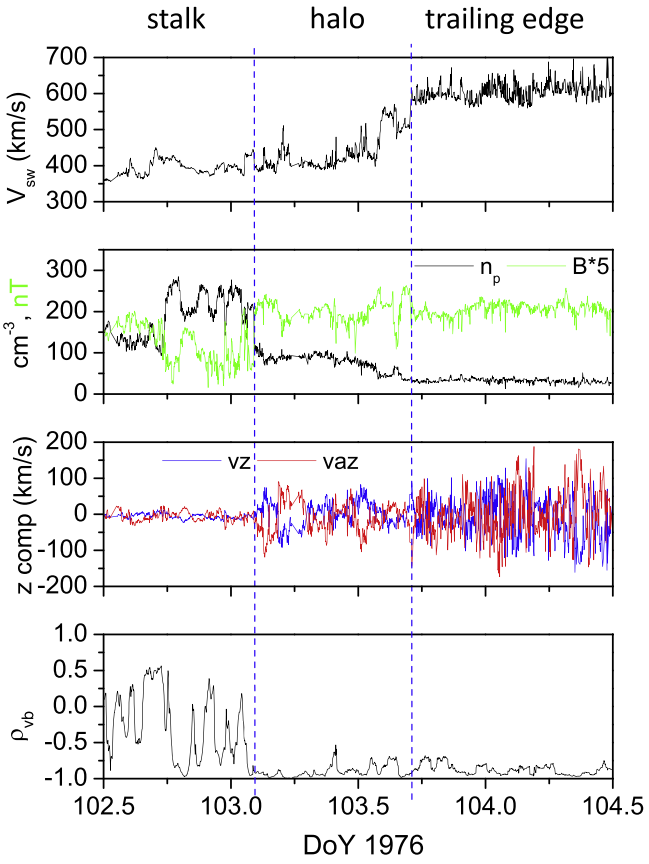

Figure 2. From top to bottom: solar wind speed V_{sw}, proton number density n_p (black) and magnetic field intensity B (green), z components of velocity v_z (blue) and magnetic field in Alfvén units v_{az} (red), and the v–b correlation coefficient of the z component ρ_{vb} at 0.3 AU.

density, obtained from IPS measurements, and in situ measurements by *Helios 2* when the s/c was around 0.3 AU from the Sun. The same authors recognized that in situ observations were the interplanetary counterpart of the streamer stalk region, which is the narrow region in the middle of the streamer belt and which underlies the heliospheric current sheet. The stalk has the highest density fluctuations and the lowest solar wind speeds. Actually, the density bumps are embedded in a density halo, a region with slightly higher density than the ambient. Looking carefully at the plots, we can actually distinguish three different regions marked by blue dashed vertical lines: the stalk until DoY 103.09, the halo until DoY 103.71, and the trailing edge of the fast stream. Alfvénic correlations develop when passing through the interface between stalk and halo. Within the halo they have a smaller amplitude if compared to the correlations within the trailing edge of the fast stream. In any case, the correlation coefficient has the same level in both regions.

Figure 3 shows a schematic representation of what happens if we project back our measurements onto the Sun surface. During this time interval the s/c is moving from negative to positive latitudes and the plots on the right-hand side show the corresponding in situ measurements by *Helios 2* at 0.3 AU. The plots on the right show, from right to left, the z components of velocity and magnetic field (in Alfvén units), the number density, and the solar wind velocity versus latitude, respectively. At very low latitudes, when the s/c crosses the stalk of the heliospheric current sheet, we observe the highest density enhancements. In this region we do not observe Alfvénic correlations. When the s/c overcomes the interface between the stalk and halo, Alfvénic correlations appear and maintain a high level of correlations, with the only difference in the amplitude of the fluctuations which becomes larger within the fast stream rather than in the halo.

3. STATISTICAL ANALYSIS—SOLAR CYCLE 23

In the previous section we showed that not only fast streams but also slow wind can be highly Alfvénic. However, this consideration should be restricted to a limited region bordering the meridional extension of polar coronal holes. *Helios* showed that the Alfvénic character of the slow wind fluctuations can be observed as far as dynamic interactions between fast and slow wind have not yet developed. In other words, the single-case study described in the previous section suggests that compressive phenomena, not only velocity shears (Coleman 1968; Roberts et al. 1987a), govern the observed radial decrease of the Alfvénicity of solar wind fluctuations (Bruno & Bavassano 1991; Grappin et al. 1991; Marsch 1991; Bavassano et al. 2000).

To make this conclusion more robust on a statistical basis, we performed an extended study embracing different phases of the solar cycle 23. We chose this specific cycle because of previous findings by D'Amicis et al. (2011), who found evidence of a peculiar behavior of solar wind turbulence in that cycle. They found that the maximum of solar cycle 23 is largely dominated by slow wind as expected, which, however, shows a high degree of Alfvénicity comparable or even higher than that found in the fast wind during the minimum of the same cycle. This is a puzzling result that will be investigated in the next sections.

We extended the study by D'Amicis et al. (2011) to a larger data set that is more representative of the particular phase of the solar cycle under study. To do this, we selected 30 months of 1 minute data from the OMNI data set at both solar maximum and minimum. In particular, we focused on DoY 1/2000 to 181/2002 at solar maximum and on DoY 182/2005 to 365/2007 at solar minimum, as indicated in Figure 4, which displays the behavior of the monthly sunspot number during cycle 23.

3.1. Method of Analysis

Following Tu & Marsch (1995), we used the normalized cross-helicity and the normalized residual energy to characterize the state of turbulence from a statistical point of view. The normalized cross-helicity, studied for the first time in the solar wind framework by Matthaeus & Goldstein (1982), is defined as

$$\sigma_C = \frac{e^+ - e^-}{e^+ + e^-} \quad (1)$$

and the normalized residual energy, first used with solar wind data by Roberts et al. (1987a), is defined as

$$\sigma_R = \frac{e^v - e^b}{e^v + e^b}. \quad (2)$$

In Equation (1), e^+ and e^- are the energy per unit mass associated with the z^+ and z^- modes (the Elsässer variables), respectively. The Elsässer variables, which are a useful tool to study Alfvénic fluctuations, are defined in the following way

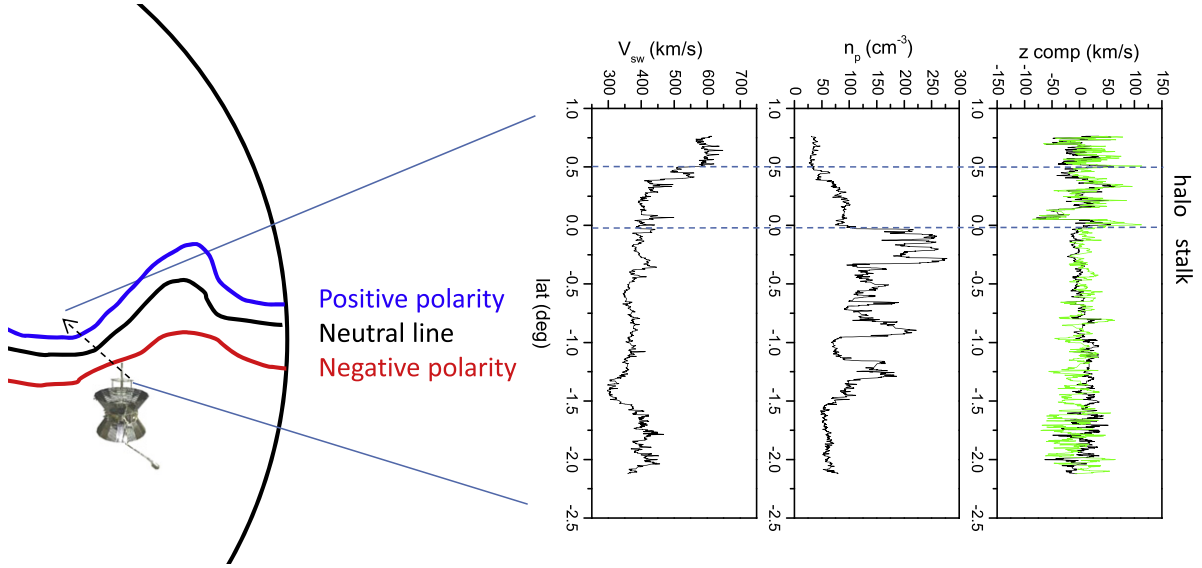

Figure 3. Schematic representation of the crossing of the current sheet on the Sun surface. The s/c is moving from negative to positive latitudes. The plots show, from left to right, the behavior of solar wind velocity V_{sw}, proton number density n_p, and z components of velocity and magnetic field (in Alfvén units) vs. latitude.

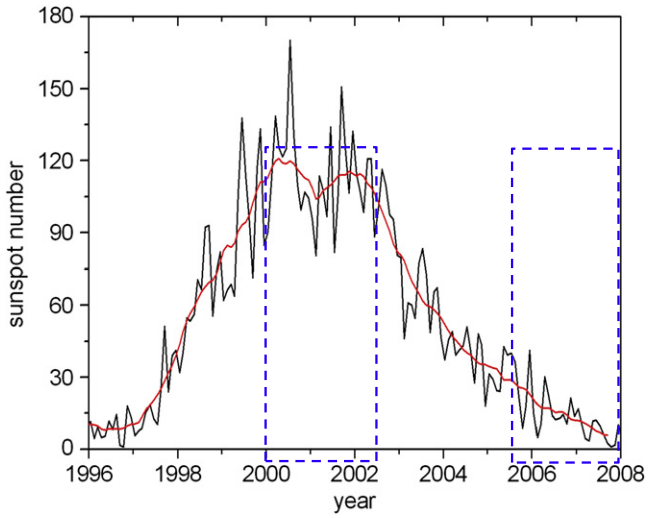

Figure 4. Monthly sunspot number as a function of time (black line) and smoothed average (red line). The dashed boxes correspond to the selected time intervals: 30 months of 1 minute-averaged data from the OMNI data set, both at solar maximum (DoY 1/2000-181/2002) and minimum (DoY 182/2005-365/2007), respectively.

(Elsässer 1950): $\boldsymbol{z}^{\pm} = \boldsymbol{v} \pm \boldsymbol{b}$, where $\boldsymbol{b}$ is the magnetic field expressed in Alfvén units ($\boldsymbol{b} = \boldsymbol{B}/(4\pi\rho)^{1/2}$, where ρ is the mass density). The sign in front of b is given by $\mathrm{sign}(-k \cdot B_0)$, where $\boldsymbol{k}$ is the wave vector and B_0 is the ambient magnetic field. In fact, for a field directed outward (with respect to the Sun), a negative correlation indicates a mode propagating away from the Sun, while a positive one represents a mode directed toward the Sun. In case the field is directed toward the Sun, the correlation sign reverses with respect to the previous cases. However, it is more convenient to define Elsässer variables in such a way that z^+ always refers to outward modes while z^- refers to inward modes. To do this, one has to rotate the magnetic field by 180° ($\boldsymbol{b} \rightarrow -\boldsymbol{b}$) every time it is directed toward the Sun (Roberts et al. 1987a; Bruno & Bavassano 1991; Grappin et al. 1991). See also Tu & Marsch (1995) and Bavassano et al. (1998) for a thorough explanation.

Equation (2) is written in terms of e^v and e^b, which are the kinetic and magnetic energy per unit mass, respectively.

σ_C was computed considering the fact that e^+ corresponds to the z^+ variance (similarly e^- corresponds to the z^- variance). The variance was computed at 1 hr scales as solar wind fluctuations show a strong Alfvénic character at this scale (Tu & Marsch 1995). In the same way, σ_R was computed by evaluating e^v and e^b, i.e., the $\boldsymbol{v}$ and $\boldsymbol{b}$ variances, respectively.

The estimates of σ_C and σ_R vary from −1 and +1. The value of σ_C is 1 (−1) when only an outward (inward) mode is present so that it indicates how much a mode (either inward or outward) is dominant with respect to the other. Absolute values of σ_C below 1 correspond to the presence of non-Alfvénic fluctuations in the solar wind parameters. σ_R is a measure of the excess magnetic energy (in Alfvén units) with respect to kinetic energy (normalized to the total energy) or vice versa, depending on the sign. The absence of magnetic (kinetic) fluctuations corresponds to σ_R equal to +1 (−1), while equipartition gives $\sigma_R = 0$, as expected for Alfvénic fluctuations.

Moreover σ_C and σ_R are linked to the correlation coefficient being $\rho_{vb} = \sigma_C \Big/ \sqrt{1 - \sigma_R^2}$, provided that σ_R is not equal to ±1. This means that σ_C is a measure of $v - b$ correlation only if σ_R is much smaller than 1, i.e., near equipartition.

3.2. Observations

The first results of this statistical analysis refer to the study of the normalized cross-helicity and residual energy as shown in Figure 5. The black circle represents the locus showing the most correlated measurements, given by $\sigma_C^2 + \sigma_R^2 = 1$, with ρ_{vb} being linked to σ_C and σ_R as shown in the previous section. At both solar minimum and maximum, the distribution extends over only one quadrant, i.e., $\sigma_C > 0$ and $\sigma_R < 0$, meaning there is a predominance of outward fluctuations showing some magnetic excess, as already found by Bruno et al. (1985) and Bavassano et al. (1998, 2000). D'Amicis et al.

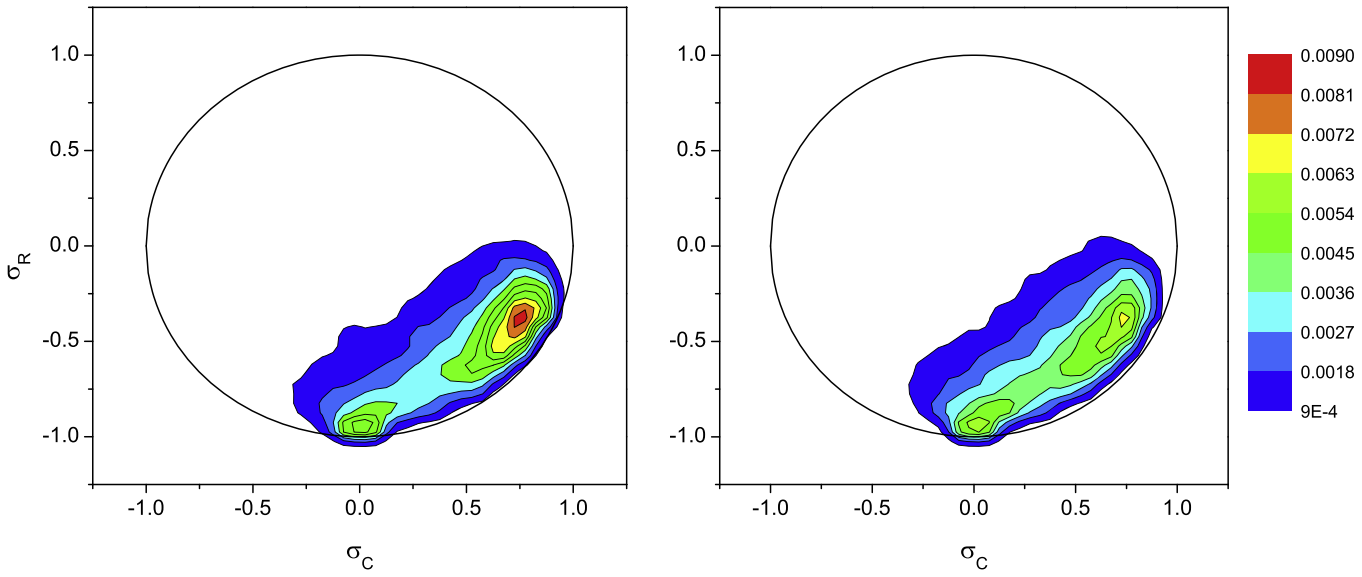

Figure 5. 2D histograms of σ_C–σ_R at the maximum (left) and minimum (right) of solar cycle 23. The color scale indicates the occurrence frequency normalized to the total number of events.

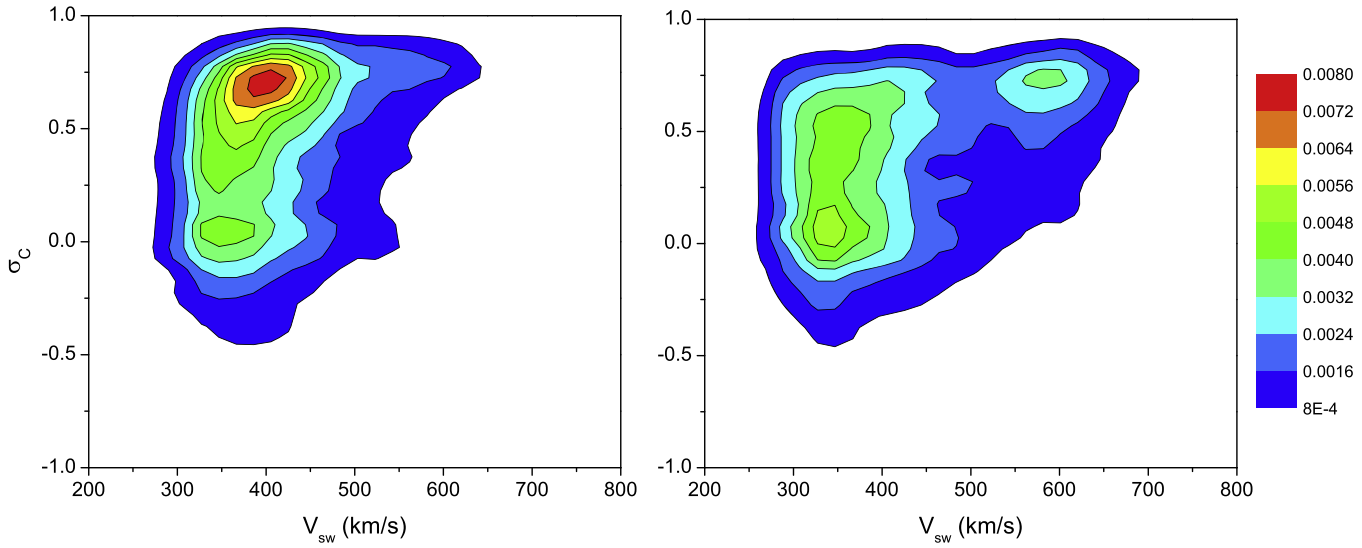

Figure 6. 2D histograms of σ_C vs. velocity at maximum (left) and minimum (right) of solar cycle 23. The color scale indicates the occurrence frequency normalized to the total number of events.

(2007, 2009, 2010) analyzed different solar cycles and found that distributions at solar minimum and maximum are remarkably different with a pronounced peak corresponding to Alfvénic fluctuations at the minimum of solar cyle 22, along with a tail toward $\sigma_C \sim 0$ and $\sigma_R \sim 1$, as already found in Bavassano et al. (1998). The latter population is however more pronounced at the maximum of solar cycle 21.

During solar cycle 23, on the contrary (Figure 5), at solar minimum, the two populations corresponding to Alfvénic fluctuations (high σ_C and low σ_R) and magnetically dominated structures, respectively, have the same statistical weight. At solar maximum, however, a robust predominance of Alfvénic fluctuations is observed. This finding is rather at odds with previous results reported in the literature so far (e.g., D'Amicis et al. 2007), suggesting that we should expect more Alfvénic solar wind fluctuations during solar minima because of the increased presence in the ecliptic of the fast wind coming from the meridional extensions of polar coronal holes.

These results stimulate the question of which is the contribution of the fast and slow wind in the two phases of the solar cycle. As a first step, we analyze the dependence of σ_C on velocity as shown in Figure 6. During solar minimum (right-hand side panel) the fast wind is characterized, as expected, by a narrow Alfvénic population while the slow wind shows a major non-Alvénic population (σ_C around zero) together with a wide spread of positive values of σ_C. During solar maximum (left-hand side panel), a predominance of slow wind is observed, as expected. However, interestingly enough, this slow wind shows the presence of a dominant Alfvénic population together with a minority of non-Alfvénic fluctuations. These results, in contrast with general expectations (e.g., Bruno & Carbone 2013), support and make statistically more robust the previous inferences by D'Amicis et al. (2011). As a matter of fact, this study is representative of the statistical behavior of the whole maximum of solar cycle 23 and not only of the short time interval considered in D'Amicis et al. (2011).

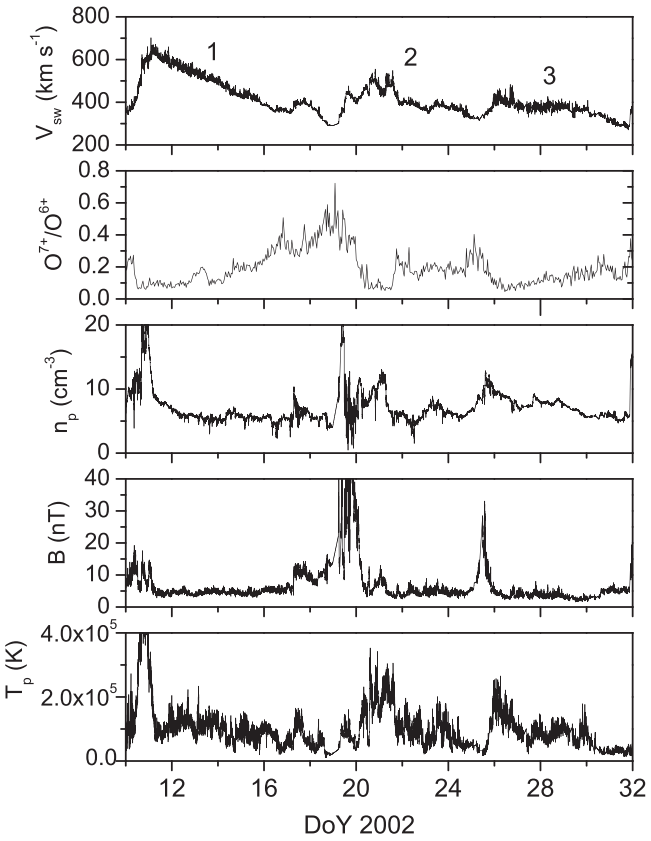

Figure 7. Time series of the selected time interval at solar maximum. Shown from top to bottom: solar wind velocity V_{sw}, O^{7+}/O^{6+} ratio, B magnitude, proton number density n_p, and proton temperature T_p. Labels 1, 2, and 3 identify the three events under study.

4. ORIGIN OF THE SLOW SOLAR WIND

We examined the whole data set from Carrington rotation 1958–1991 and found, in about 70% of the cases, intervals of Alfvénic slow solar wind. Since there are too many intervals to be shown in this paper, we decided to show only a representative example, i.e., from DoY 10/2002 to DoY 31/2002. This particular interval, like many others, clearly shows the presence of two different slow wind types.

Figure 7 shows the time series of some parameters for the representative time interval. Elemental composition data are obtained from the SWICS experiment on board *ACE* s/c available at 1 hr resolution. Looking at the different parameters (from top to bottom, the bulk velocity, O^{7+}/O^{6+} charge state ratio, proton number density, proton temperature, and B magnitude) we can identify three different events: the one labeled "1" corresponds to an interval of fast wind while "2" and "3" correspond to slow wind. The parameter that better discriminates between fast and slow wind source regions is the O^{7+}/O^{6+} ratio. High values are found within the slow wind from coronal streamers while low values are found in the fast wind coming from coronal holes (as already found by Geiss et al. 1995). In this plot we clearly observe that higher values of this ratio characterize event 2 while events 1 and 3 have similar characteristics (also considering the larger fluctuation amplitudes in velocity, for example). Moreover, although during events 2 and 3 the speed value is roughly constant, the amount of O^{7+}/O^{6+} is different. For this reason we identify event 2 as "slow wind 1st type" while event 3 as "slow wind 2nd type."

The different values of the O^{7+}/O^{6+} ratio is an indication that we are observing plasma coming from different source regions that we can localize by mapping back the measurements corresponding to the three events onto a synoptic map during Carrington rotation 1985, as shown in Figure 8. The arrows indicate the beginning of the three events along with the different magnetic field polarities encountered by the s/c (plus and minus sign). The coronal magnetic field shown in Figure 8 is extrapolated from photospheric field observations using a potential field model (Altschuler & Newkirk 1969; Schatten et al. 1969; Wilcox et al. 1980; Hoeksema et al. 1983). The field is forced to be radial at the source surface (assumed to be at 2.5 solar radii). Here, blue light shading shows the positive regions while the red ones show negative regions. The neutral line is black. By projecting back our solar wind measurements (with a rough estimate assuming a constant and radial velocity) on the solar surface we find that events 1 and 3 come from the meridional extensions of the polar coronal holes characterized by open field line regions while event 2 comes from a source region, limited in extension and characterized by a more complex field line topology. It is rather interesting to note that slow wind type 2 shows plasma features quite similar to those pertaining to the fast wind (interval 1).

Our finding supports results by Antonucci et al. (2005) who, using UVCS observations, found evidence for the existence of two kinds of slow solar wind typically originating from different source regions, coronal streamers, and coronal holes' boundaries, respectively. We examined all the synoptic maps from Carrington rotations 1958–1991 and found very stable magnetic configurations during successive solar rotations. Moreover, recent studies by Platten et al. (2014) found a remarkable number of localized coronal holes at all latitudes during the maximum of cycle 23, supporting our findings on a statistical basis. In conclusion, we can unambiguously identify the slow wind of 1st type as the "classical" slow wind coming from coronal streamers while the 2nd type is the "anomalous" slow wind coming from the boundaries between closed and open magnetic field regions, which have characteristics more similar to fast wind than classical slow wind.

5. ON THE ROLE OF COMPRESSIBILITY

Why are magnetic field and plasma fluctuations in these two kinds of slow wind so different in their Alfvénic character? Does it depend on the different magnetic field topology at the source regions or on more accessible intrinsic features of these fluctuations which we can measure in situ? Following Bruno & Bavassano (1991), who suggested that compressible phenomena play an important role in determining the Alfvénic character of solar wind fluctuations, we add to our analysis another relevant element such as fluctuation compressibility. To do this we compute number density and magnetic field compressibility as in Bruno & Bavassano (1991). The former is defined as:

$$C_\rho = \left(\sigma_\rho^2 / \langle\rho\rangle^2\right)^{1/2} \tag{3}$$

with σ_ρ^2 the variance of ρ and $\langle\rho\rangle$ the average value computed over 1 hr. The latter is defined as:

$$C_{bi} = \left(\sigma_B^2 \Big/ \sum_i \sigma_{bi}^2\right)^{1/2} \tag{4}$$

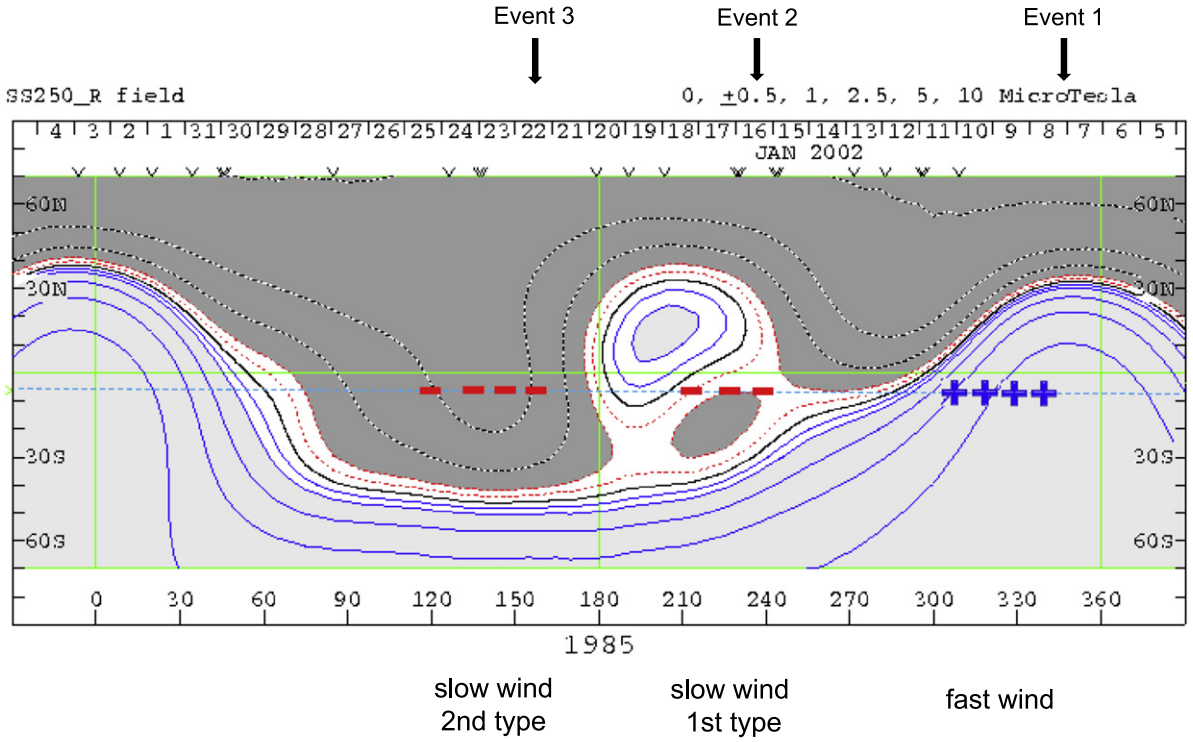

Figure 8. Synoptic map of Carrington rotation 1985. The arrows indicate the beginning of the three time periods (events labeled "1," "2," and "3"). Superimposed plus and minus signs indicate different magnetic field polarities detected by the s/c. Blue light shading shows the positive regions while the red ones show negative regions. Black is the neutral line.

with σ_B^2 and σ_{bi}^2 the variance of the B magnitude and of each magnetic field component (with $i = x, y, z$), respectively, computed over 1 hr.

Figure 9 shows these parameters for the selected time interval already shown in Figure 7 along with V_{sw}, σ_C and, the e^+ and e^- modes. The cross-helicity σ_C shows similar high levels within events 1 and 3 while event 2 is characterized by lower values. At the same time, e^- maintains almost the same level throughout the time interval so that a depletion of σ_C corresponds to a decrease of e^+ rather to an increase of e^-, as already stated in Bruno & Bavassano (1991). Moreover there is no clear relationship with density compressibility since this parameter maintains almost the same level throughout the time interval considered, fluctuating around 10%. On the contrary we observe on average a lower value of magnetic field compressibility in events 1 and 3 rather than in event 2, suggesting a more relevant role of magnetic compressibility with respect to density fluctuations.

From a statistical point of view, the link between σ_C and compressibility can be searched for in the 2D histograms of Figure 10 built for the maximum and minimum phases of cycle 23. During solar maximum, the two distributions in the upper and lower panels show an enhanced peak for high and positive values of σ_C and low compressibility level. A light tail for each distribution also extends toward low σ_C values revealing a possible link only with field compressibility which increases with decreasing σ_C. During solar minimum (see right-hand side panels), the distributions are much less peaked revealing that high σ_C values are much less dominant and, again, a possible anticorrelation is confirmed only by field compressibility. Summarizing these last results, we can state that the highest values of σ_C are coupled to the lowest values of field

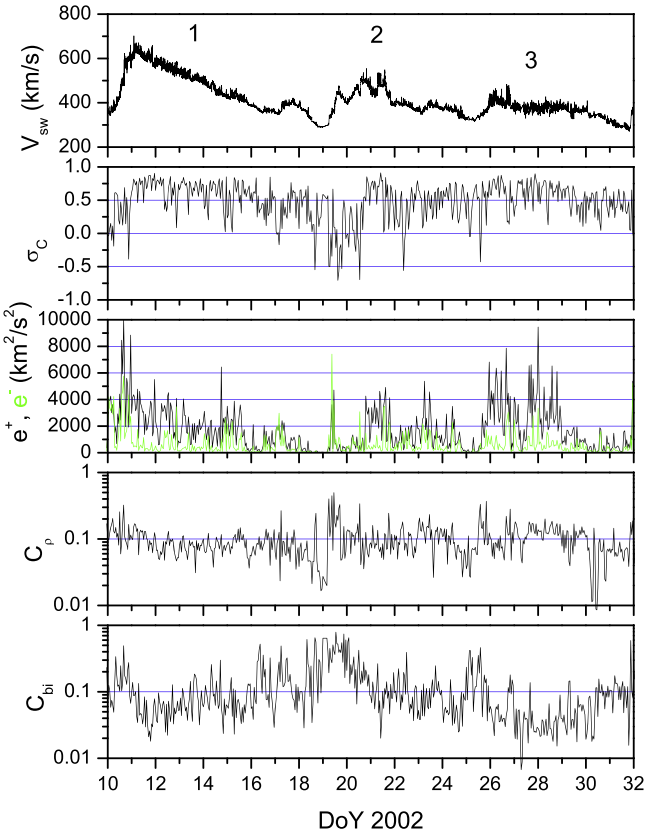

Figure 9. Time series of the selected time interval at solar maximum. Shown from top to bottom: solar wind velocity V_{sw}, normalized cross-helicity σ_C, e^+ (black) and e^- (green), density compressibility C_ρ, and B compressibility C_{bi}. Labels "1," "2," and "3" identify the three events under study.

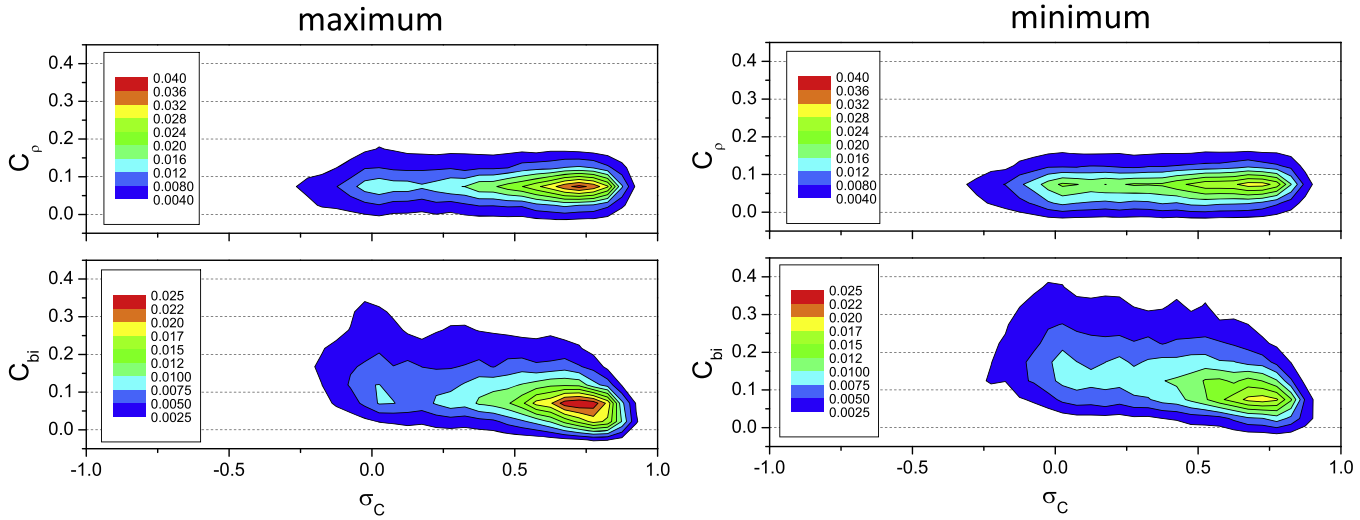

Figure 10. 2D histograms of σ_C vs. compressibility (upper and lower panels with density and magnetic field compressibility, respectively) at the maximum (left) and minimum (right) of solar cycle 23. The color scale indicates the occurrence frequency normalized to the total number of events.

compressibility, that wind fluctuations during the maximum of cycle 23 were less affected by compressive phenomena and, as a consequence, the maximum of this cycle was more Alfvénic than its corresponding minimum.

6. SUMMARY

The solar wind generally transports Alfvénic fluctuations frozen in it. It is very common to find these fluctuations and the best examples are found within the fast solar wind. This wind comes from open field line regions identified as polar coronal holes from where it is easy for these fluctuations, which propagate along the local mean field, to escape toward the interplanetary space. On the contrary, a completely different situation is experienced by these fluctuations within the slow wind, generally characterized by mostly closed field regions around local current sheets. Our results, reported for the first time in the literature, show the existence in the interplanetary space of two types of slow solar wind of different origin: the classical one, or 1st type, coming from coronal streamers or active regions, characterized by non-Alfvénic fluctuations and the anomalous one, or 2nd type, originating from the boundary of coronal holes. This 2nd type of slow wind shows the same level of Alfvénic correlations found in the nearby fast wind but of considerably smaller amplitude. Moreover, similar to the nearby fast and Alfvénic region, this wind is also characterized by a remarkably low compressibility when observed close to the Sun.

In our single-case study relative to a fast stream observed at 0.3 AU, we showed that when the wind expands and dynamic interaction starts to build up, the Alfvénicity of this slow wind region is progressively destroyed. As a matter of fact, magnetic field compressibility rather than number density fluctuations or velocity shear mechanism governs the Alfvénicity level of these slow wind regions.

These observations were at the basis of a wider statistical study dedicated to unraveling the causes of the unexpected high Alfvénicity of the fluctuations during the maximum phase of solar cycle 23. As a matter of fact, interplanetary fluctuations during this particular phase are highly Alfvénic, more than the corresponding fluctuations observed during the following minimum, although the wind was not populated by high speed streams like it was during the minimum. On the other hand, our study highlighted, together with their remarkable Alfvénicity, the very low compressibility level of these fluctuations confirming on a wider statistical basis the role of compressions and similar findings by D'Amicis et al. (2011).

The authors are grateful to the following people and organizations for the provision of data used in this study: N. Papatashvilli and NASA/GSFC for the use of OMNI data (both plasma and magnetic field); H. R. Rosenbauer and Max-Planck-Institut fur Aeronomie for the use of data from the *Helios*/E1 plasma experiment, and N. F. Ness and the Bartol Research Institute for the use of the magnetometers aboard the *Helios 2* spacecraft. Solar magnetic field maps at the source surface are available from http://wso.stanford.edu/. The present work has been supported by the Italian Space Agency (ASI) under contract I/013/12/0 ASI/INAF.

REFERENCES

Altschuler, M. D., & Newkirk, G., Jr 1969, SoPh, 9, 131
Antonucci, E., Abbo, L., & Dodero, M. A. 2005, A&A, 435, 699
Bavassano, B., & Bruno, R. 1989, JGR, 94, 168
Bavassano, B., & Bruno, R. 1989, JGR, 94, 11977
Bavassano, B., Dobrowolny, M., Mariani, F., & Ness, N. F. 1982, JGR, 87, 3617
Bavassano, B., Pietropaolo, E., & Bruno, R. 1998, JGR, 103, 6521
Bavassano, B., Pietropaolo, E., & Bruno, R. 2000, JGR, 105, 12697
Bavassano, B., Woo, R., & Bruno, R. 1997, GeoRL, 24, 1655
Belcher, J. W., & Davis, L. 1971, JGR, 76, 3534
Bruno, R., & Bavassano, B. 1991, JGR, 96, 7841
Bruno, R., & Carbone, V. 2013, LRSP, 10, 2
Bruno, R., Bavassano, B., & Villante, U. 1985, JGR, 90, 4373
Bruno, R., D'Amicis, R., Bavassano, B., Carbone, V., & Sorriso-Valvo, L. 2007, AnGp, 25, 1913
Coleman, P. J. 1968, ApJ, 153, 371
D'Amicis, R., Bruno, R., & Bavassano, B. 2007, GeoRL, 34, L05108
D'Amicis, R., Bruno, R., & Bavassano, B. 2009, JASTP, 71, 1014
D'Amicis, R., Bruno, R., & Bavassano, B. 2010, AdSpR, 46, 514
D'Amicis, R., Bruno, R., & Bavassano, B. 2011, JASTP, 3, 653
Dobrowolny, M., Mangeney, A., & Veltri, P. 1980, PhRvL, 45, 144
Elsässer, W. M. 1950, PhRv, 79, 183
Geiss, J., Glockler, G., & von Steiger, R. 1995, SSRv, 72, 49
Goelzer, M. L., Schwadron, N. A., & Smith, C. W. 2014, JGRA, 119, 115

Grappin, R., & Velli, M. 1996, JGR, 101, 425
Grappin, R., Velli, M., & Mangeney, A. 1991, AnGp, 9, 416
Hoeksema, J. T., Wilcox, J. M., & Scherrer, P. H. 1983, JGR, 88, 9910
Hundhausen, A. J. 1972, in Physics and Chemistry in Space, Vol. 5, ed. J. G. Roederer (Berlin: Springer), 238
Marsch, E. 1991, in Physics and Chemistry in Space, Vol. 21, ed. R. Schwenn & E. Marsch (Berlin Heidelberg: Springer), 159
Matthaeus, W. H., & Goldstein, M. l. 1982, JGR, 87, 6011
Matthaeus, W. H., Minnie, J., Breech, B., Parhi, S., Bieber, J. W., & Oughton, S. 2004, GeoRL, 31, L12803
Phillips, J. L., Bame, S. J., Feldman, W. C., et al. 1995, Sci, 268, 1030
Platten, S. J., Parnell, C. E., Haynes, A. L., Priest, E. R., & Mackay, D. H. 2014, A&A, 565, A44
Roberts, D. A., Goldstein, M. L., Klein, L. W., & Matthaeus, W. H. 1987b, JGR, 92, 12023
Roberts, D. A., Klein, L. W., Goldstein, M. L., & Matthaeus, W. H. 1987a, JGR, 92, 11,021
Schatten, H., Wilcox, J. M., & Ness, N. F. 1969, SoPh, 6, 442
Tu, C.-Y., & Marsch, E. 1993, JGR, 98, 1257
Tu, C.-Y., & Marsch, E. 1995, SSRv, 73, 1–210
Tu, C.-Y., Marsch, E., & Thieme, K. M. 1989, JGR, 94, 11739
Wilcox, J. M., Hoeksema, J. T., & Scherrer, P. H. 1980, Sci, 209, 603